Dispersion relation and growth rate for a corrugated channel free-electron laser with a helical wiggler pump

A. Hasanbeigi† and H. Mehdian

Department of Physics and Institute for Plasma Research, Kharazmi University, 49 Dr Mofatteh Avenue, Tehran 15614, Iran

(Received 9 October 2012; revised manuscript received 4 March 2013)

The effects of corrugated ion channels on electron trajectories and spatial growth rate for a free-electron laser with a one-dimensional helical wiggler have been investigated. Analysis of the steady-state electron trajectories is performed by solving the equations of motion. Our results show that the presence of a corrugated channel shifts the resonance frequency to smaller values of ion channel frequency. The sixth-order dispersion equation describing the coupling between the electrostatic beam mode and the electromagnetic mode has also been derived. The dispersion relation characteristic is analyzed in detail by numerical solution. Results show that the growth rate of instability in the presence of corrugated ion channels can be greatly enhanced relative to the case of an uniform ion channel.

Keywords: corrugated ion-channel free-electron laser, growth rate, helical wiggler

PACS: 52.59.Rz, 41.60.Cr, 52.27.Ny **DOI:** 10.1088/1674-1056/22/7/075205

1. Introduction

Ion-channel guiding (ICG) in free-electron lasers (FELs) has been a subject of great interest in two decades.[1–5] If an intense relativistic electron beam is injected into a neutral plasma in a blow-out regime, when the electron beam density is higher than the plasma density, plasma electrons are ejected electrostatically by the beam space charge. The beam electrons are then electrostatically attracted by the positive ions. It is well known that an electron beam is guided through the channel in the ion focused regime. The presence of ions neutralizes the beam space charge, and thus overcomes the beam divergence generated by its self-fields. This technique can eliminate the need for conventional focusing magnets, thereby reducing the capital and running cost.[1] Also it permits beam currents higher than the vacuum limit and helps radiation guiding.[6] The ICG was employed in FEL amplification experiments after successful demonstration of the proceeding beam transport experiment.[7] Several theoretical studies indicate that ICG may offer some distinct advantages.[8–14] The corrugated ion channel can be created by three methods. It could be generated by beam-induced ionization of axially periodic gas puffs,[15] by a large number of laser beamlets incident perpendicular to the electron beam, or by a surface flashover plasma source coupled to the beam pulsed power source.[15–17] The periodic ion channel is similar to a uniform ion-channel guiding, in that no magnetic field is required but it causes more effective transverse oscillations and there is a corresponding strong interaction between the electrons and an electromagnetic wave. Therefore, a periodic ion channel may be used to guide electron beams and to excite its transverse oscillations over distances on the order of several betatron lengths of the beam.[16] The effects of periodic ion channels on the gain of FEL with helical wiggler have also been investigated.[18] The purpose of the present paper is to investigate the effects of periodic ion channels on the electron trajectories and the growth rate.

This paper is organized as follows. In Section 2, the relativistic motion of a single electron in the presence of a helical wiggler and period ICG is formulated, and the steady-state solution of the equation of motion is then derived for group-I and group-II orbits. The coupled dispersion relation of the longitudinal and transverse modes is obtained in Section 3. Section 4 is devoted to numerical results, and Section 5 ends with conclusions.

2. Steady-state trajectories

Consider the electron dynamics in a configuration which consists of a helical wiggler and a periodic ion channel guiding, whose density is given in the laboratory frame for $z > 0$ by

$$n_{\rm i}(z) = \frac{n_{\rm i}}{2}(1+\cos k_{\rm i} z), \tag{1}$$

where z is the axial coordinate, and $k_{\rm i} = 2\pi/\lambda_{\rm i}$ is the undulator wave number. The wiggler field may be described in term of one-dimensional approximation by

$$\boldsymbol{B}_{\rm w} = B_{\rm w}[\boldsymbol{e}_x \cos k_{\rm w} z + \boldsymbol{e}_y \sin k_{\rm w} z], \tag{2}$$

where $B_{\rm w}$ is the amplitude, and $k_{\rm w}$ is the wiggler magnetic field wave number.

The electrostatic electric field generated by a periodic ion channel, with its axis coincident with the wiggler z axis in cylindrical coordinates, may be written as[15]

$$\begin{aligned}\boldsymbol{E}_{\rm i}(r,z) \;=\; & \pi e n_{\rm i} r[1+2{\rm K}_1(k_{\rm i} r){\rm I}_1(k_{\rm i} r)\cos k_{\rm i} z]\boldsymbol{e}_{\rm r} \\ & + \frac{2\pi e n_{\rm i}}{k_{\rm i}}[1-k_{\rm i} r{\rm K}_1(k_{\rm i} r){\rm I}_0(k_{\rm i} r)]\sin k_{\rm i} z \boldsymbol{e}_z, \end{aligned} \tag{3}$$

†Corresponding author. E-mail: hbeigi@tmu.ac.ir

© 2013 Chinese Physical Society and IOP Publishing Ltd

where I_n and K_n denote the modified Bessel function of the first and second kinds, respectively. For the sake of clarity of presentation, it is useful to consider the idealized one-dimensional approximation in which the electron displacement from the axis of symmetry remains much less than the wiggler period (i.e., $r \ll \lambda_w$). When the wiggler period greatly exceeds the beam radius, the wiggler field is mostly radial. In this limit, the electrostatic field can be given in a particularly simple form

$$\boldsymbol{E}_i = \pi e n_i (1+\cos k_i z)(x\boldsymbol{e}_x + y\boldsymbol{e}_y). \tag{4}$$

The electron orbits in such a case are determined by the Lorentz force equation

$$\frac{\mathrm{d}(\boldsymbol{v})}{\mathrm{d}t} = \frac{-e}{\gamma m}\left[\left(\boldsymbol{I} - \frac{1}{c^2}\boldsymbol{v}\boldsymbol{v}\right)\cdot\boldsymbol{E}_i + \frac{1}{c}\boldsymbol{v}\times\boldsymbol{B}_w\right], \tag{5}$$

$$\frac{\mathrm{d}\gamma}{\mathrm{d}t} = -\frac{e}{mc^2}\boldsymbol{v}\cdot\boldsymbol{E}_i, \tag{6}$$

where e, m, and $\boldsymbol{v}$ denote the charge, mass, and velocity of an electron, respectively. The Lorentz factor corresponding to velocity $\boldsymbol{v}$ is $\gamma = (1-v^2/c^2)^{1/2}$. For convenience, we introduce the wiggler frame as

$$\boldsymbol{e}_1 = \boldsymbol{e}_x \cos k_w z + \boldsymbol{e}_y \sin k_w z, \tag{7}$$

$$\boldsymbol{e}_2 = -\boldsymbol{e}_x \sin k_w z + \boldsymbol{e}_y \cos k_w z, \tag{8}$$

$$\boldsymbol{e}_3 = \boldsymbol{e}_z. \tag{9}$$

The scalar equations of motion in the wiggler frame can be written as

$$\frac{\mathrm{d}\beta_1}{\mathrm{d}\tau} = \frac{\omega_i^2}{2}(1+\cos\bar{k}_i\chi_3)[-(1-\beta_1^2)\chi_1 + \beta_1\beta_2\chi_2] + \beta_2\beta_3, \tag{10}$$

$$\frac{\mathrm{d}\beta_2}{\mathrm{d}\tau} = \frac{\omega_i^2}{2}(1+\cos\bar{k}_i\chi_3)[-(1-\beta_2^2)\chi_2 + \beta_1\beta_2\chi_1] - \beta_1\beta_3 - \Omega_w\beta_3, \tag{11}$$

$$\frac{\mathrm{d}\beta_3}{\mathrm{d}\tau} = \frac{\omega_i^2}{2}(1+\cos\bar{k}_i\chi_3)\beta_3(\beta_1\chi_1 + \beta_2\chi_2), \tag{12}$$

$$\frac{\mathrm{d}\gamma}{\mathrm{d}\tau} = -\gamma\frac{\omega_i^2}{2}(1+\cos\bar{k}_i\chi_3)(\beta_1\chi_1 + \beta_2\chi_2). \tag{13}$$

In these equations, the quantities are normalized as $\Omega_w \equiv eB_w/mc^2k_w\gamma$, which is the normalized wiggler magnetic field, $\omega_i \equiv (2\pi e^2 n_i/\gamma mc^2 k_w^2)^{1/2}$ is the normalized ion-channel frequency, $\beta_i = v_i/c$, $\chi_i = k_w x_i$, $\tau = ck_w t$, and $\bar{k}_i = k_i/k_w$. The relations between the normalized transverse position coordinates in the wiggler frame and the normalized velocity components are given by

$$\beta_1 = \frac{\mathrm{d}\chi_1}{\mathrm{d}\tau} - \beta_3\chi_2, \tag{14}$$

$$\beta_2 = \frac{\mathrm{d}\chi_2}{\mathrm{d}\tau} + \beta_3\chi_1. \tag{15}$$

The steady-state orbits ($\gamma = \gamma_0 = \text{const}$) for this configuration are expressed as

$$\beta_1 = \frac{\beta_\parallel^2\Omega_w}{\omega_i^2(1+\cos\bar{k}_i\chi_3) - \beta_\parallel^2}, \tag{16}$$

$$\beta_2 = 0, \quad \beta_3 = \beta_\parallel = \text{const}, \tag{17}$$

and

$$\chi_1 = 0, \quad \chi_2 = -\frac{\beta_1}{\beta_\parallel}, \quad \chi_3 = \beta_\parallel\tau. \tag{18}$$

Substituting Eqs. (16) and (17) into $1-\beta_3^2-\beta_1^2-\gamma^{-2} = 0$ and averaging over L, the FEL length, after some straight forward algebra, yields

$$\omega_i^2 - \frac{\tan(Lk_i/2)\{\beta_3^2 + [\beta_3^2(\beta_3^2-1)\gamma^2 \pm \sec^2(Lk_i/2)\sqrt{\beta_3^4\gamma^2(-\beta_3^2\gamma^2+\gamma^2-1)\Omega_w^2\cos^4(Lk_i/2)}]\}}{L(\beta_3^2\gamma^2-\gamma^2+1)k_i} = 0. \tag{19}$$

Although it is easy to evaluate ω_i^2 from Eq. (19), once β_3 is given, the inverse problem of finding β_3 when ω_i is known can only be solved numerically.

3. Dispersion relation

3.1. Wave formulation

Analysis of the wave propagation in the wiggler with periodic ion-channel guiding will be based on the electron momentum transfer equation

$$\frac{\partial\boldsymbol{v}}{\partial t} + \boldsymbol{v}\cdot\nabla\boldsymbol{v} = -\frac{e}{m\gamma}\left[\boldsymbol{E} - \frac{1}{c^2}\boldsymbol{v}(\boldsymbol{v}\cdot\boldsymbol{E}) + \frac{1}{c}\boldsymbol{v}\times\boldsymbol{B}\right], \tag{20}$$

along with the equation of continuity

$$\nabla\cdot(n\boldsymbol{v}) + \partial n/\partial t = 0, \tag{21}$$

the Faraday law

$$\nabla\times\boldsymbol{E} = -\frac{1}{c}\frac{\partial\boldsymbol{B}}{\partial t}, \tag{22}$$

and the Ampere–Maxwell law in the form of

$$\nabla\times\boldsymbol{B} = \frac{4\pi}{c}\boldsymbol{J} + \frac{1}{c}\frac{\partial\boldsymbol{E}}{\partial t}. \tag{23}$$

The electron fluid variables and fields will be written in terms of an unperturbed part plus a small perturbation as

$$n = n_0 + n, \quad \boldsymbol{v} = \boldsymbol{v}_0 + \boldsymbol{v},$$

$$\boldsymbol{E} = \boldsymbol{E}_{\rm w} + \boldsymbol{E}_{\rm r} + \boldsymbol{E}_{\rm l} + \boldsymbol{E}_{\rm i},$$
$$\boldsymbol{B} = \boldsymbol{B}_{\rm w} + \boldsymbol{B}_{\rm r}, \tag{24}$$

where subscripts r, i, and l stand for radiation, ion, and space charge, respectively.

The Lorentz relativistic factor, γ, will be approximated by

$$\frac{1}{\gamma} = \frac{1}{\gamma_0} - \gamma_0 \frac{\boldsymbol{v}_0 \cdot \boldsymbol{v}}{c^2}. \tag{25}$$

Using Floquet's theorem, allowing the axial and time dependence of all perturbed parameters to take the general form of

$$F = \sum_{n=-\infty}^{n=+\infty} f_n \, {\rm e}^{{\rm i}(k_n z - \omega t)}, \tag{26}$$

where $k_n = k + nk_{\rm w}$, ω and k denote the frequency and wave number of mixed, radiation and space charge, waves. Substituting Eqs. (24)–(26) into Eq. (20) and then linearizing it, we obtain

$$\begin{aligned} v_{xn} = {} & \frac{-{\rm i}e}{\gamma_0 m \Omega_n}\left[E_{{\rm r}xn} + \pi n_{\rm i} e\left(x_n + \frac{x_{n+2}+x_{n-2}}{2}\right)\right. \\ & - \beta_{0z} B_{{\rm r}yn} - \frac{\beta_{0z}\beta_{\rm w}}{2}(E_{{\rm l}n+1} + E_{{\rm l}n-1}) \\ & \left. - \frac{\pi n_{\rm i} e \beta_{\rm w}}{2\beta_{0z}}(z_{n-1} + z_{n+1} - z_{n-3} - z_{n+3})\right] + \frac{e\gamma_0}{2mc\Omega_n} \\ & \times \left[B_{\rm w}\left(\frac{1}{\gamma_0^2} - \beta_{z0}^2\right) + \frac{\pi n_{\rm i} e \beta_{\rm w} c}{k_{\rm w}\beta_{z0}}\right](v_{zn-1} - v_{zn+1}) \\ & - \frac{\pi n_{\rm i} e \beta_{\rm w} c}{2{\rm i}\beta_{z0}}(v_{zn-3} - v_{zn+3} + v_{zn-1} - v_{zn+1}), \end{aligned} \tag{27}$$

$$\begin{aligned} v_{yn} = {} & \frac{-{\rm i}e}{\gamma_0 m \Omega_n}\left[E_{{\rm r}yn} + \pi n_{\rm i} e\left(y_n + \frac{y_{n+2}+y_{n-2}}{2}\right)\right. \\ & + \beta_{0z} B_{{\rm r}xn} - \frac{\beta_{0z}\beta_{\rm w}}{2{\rm i}}(E_{{\rm l}n+1} - E_{{\rm l}n-1}) \\ & \left. - \frac{\pi n_{\rm i} e \beta_{\rm w}}{2{\rm i}\beta_{0z}}(z_{n-3} - z_{n+3} + z_{n-1} - z_{n+1})\right] \\ & - \frac{{\rm i}e\gamma_0}{2mc\Omega_n}\left[B_{\rm w}\left(\frac{1}{\gamma_0^2} - \beta_{z0}^2\right) + \frac{\pi n_{\rm i} e \beta_{\rm w} c}{k_{\rm w}\beta_{z0}}\right](v_{zn-1} + v_{zn+1}) \\ & + \frac{\pi n_{\rm i} e \beta_{\rm w} c}{2k_{\rm w}\beta_{z0}}(v_{zn-3} + v_{zn+3} + v_{zn+1} + v_{zn-1}), \end{aligned} \tag{28}$$

$$\begin{aligned} v_{zn} = {} & \frac{-{\rm i}e}{\gamma_0 m \Omega_n}\left[\frac{E_{{\rm l}n}}{\gamma_{0z}^2} + \frac{\beta_{\rm w}}{2}(B_{{\rm r}yn-1} + {\rm i}B_{{\rm r}xn-1} + B_{{\rm r}yn+1} - {\rm i}B_{{\rm r}xn+1})\right. \\ & - \frac{1}{2c}\left(B_{\rm w} - \frac{\beta_{z0}\pi n_{\rm i} e \beta_{\rm w} c}{2k_{\rm w}\beta_{z0}}\right) \\ & \times [v_{yn-1} + {\rm i}v_{xn-1} + v_{yn+1} - {\rm i}v_{xn+1}] \\ & - \frac{\beta_{\rm w}\beta_{z0}}{2}(E_{{\rm r}xn+1} + {\rm i}E_{{\rm r}yn+1} + E_{{\rm r}xn-1} - {\rm i}E_{{\rm r}yn-1}) \\ & - \frac{\beta_{z0}\pi n_{\rm i} e \beta_{\rm w}}{2}[x_{n-1} - {\rm i}y_{n-1} + x_{n+1} + {\rm i}y_{n+1}] \end{aligned}$$

$$\left. - \frac{\beta_{z0}\pi n_{\rm i} e \beta_{\rm w}}{4}[x_{n-1} - {\rm i}y_{n-1} + x_{n+1} + {\rm i}y_{n+1} + x_{n-3} - {\rm i}y_{n-3} + x_{n+3} + {\rm i}y_{n+3}]\right], \tag{29}$$

where $\Omega_n = \omega - k_n c\beta_{0z}$, $\gamma_{0z}^{-2} = 1 - \beta_{0z}^2$, and $\beta_{\rm w} = (1 - \beta_3^2 - \gamma^{-2})^{1/2}$. We suppose $k_{\rm i} = 2k_{\rm w}$.

Inserting Eq. (26) into the continuity equation, $\nabla \cdot (n\boldsymbol{v}) + \partial n/\partial t = 0$, yields

$$n_n = \frac{n_0 k_n}{\Omega_n} c\beta_{zn}. \tag{30}$$

The linearized current density takes the form of

$$\boldsymbol{J} = -e(n\boldsymbol{v}_0 + n_0\boldsymbol{v}). \tag{31}$$

Making use of Eqs. (26) and (30), the linearized perturbed current density component amplitudes may be expressed as

$$J_{xn} = -en_0 v_{xn} - \frac{en_0 c\beta_{\rm w}}{2}\left(\frac{v_{zn-1}k_{n-1}}{\Omega_{n-1,+}} + \frac{v_{zn+1}k_{n+1}}{\Omega_{n+1,-}}\right), \tag{32}$$

$$J_{yn} = -en_0 v_{yn} + \frac{{\rm i}en_0 c\beta_{\rm w}}{2}\left(\frac{v_{zn-1}k_{n-1}}{\Omega_{n-1,+}} - \frac{v_{zn+1}k_{n+1}}{\Omega_{n+1,-}}\right), \tag{33}$$

$$J_{zn} = -en_0 v_{zn}\left(1 + \frac{k_n v_{0z}}{\Omega_n}\right). \tag{34}$$

3.2. Solution of wave equation

The combination of Faraday's law and Ampere–Maxwell law gives the wave equation as

$$\nabla \times (\nabla \times \boldsymbol{E}) + \frac{1}{c^2}\frac{\partial^2 \boldsymbol{E}}{\partial t^2} + \frac{4\pi}{c^2}\frac{\partial \boldsymbol{J}}{\partial t} = 0. \tag{35}$$

Assuming the transverse oscillations to be small and with the help of Eq. (26), the above equation leads to

$$\left(k_n^2 - \frac{\omega^2}{c^2}\right)\begin{pmatrix} E_{xn} \\ E_{yn} \end{pmatrix} - \frac{4\pi{\rm i}\omega}{c^2}\begin{pmatrix} J_{xn} \\ J_{yn} \end{pmatrix} = 0, \tag{36}$$

$$-\frac{\omega^2}{c^2} - \frac{4\pi{\rm i}\omega}{c^2}J_{zn} = 0. \tag{37}$$

Substituting source currents (Eqs. (32)–(34)) and perturbed velocities (Eqs. (27)–(29)) into Eqs. (36) and (37), the dispersion equation can be cast into a substantially simpler form

$$\omega_{\rm b}^2\left(\frac{\omega_i^2}{\beta_3\bar{k}_n(2\omega - \beta_3\bar{k}_n) + \omega_i^2 - \omega^2} - \frac{A}{B} - 1\right) - \bar{k}_n^2 + \omega^2 = 0, \tag{38}$$

where

$$A = \beta_{\rm w}(\bar{k}_n + 1)\left(\frac{(\omega - \beta_3\bar{k}_n)(3\omega_i^2\beta_{\rm w}(\omega - \beta_3(\bar{k}_n + 1)) - 4\Omega_{\rm w}(\omega - \beta_3\bar{k}_n))}{\beta_3\bar{k}_n(\beta_3\bar{k}_n - 2\omega) - \omega_i^2 + \omega^2} + 4\beta_{\rm w}(\bar{k}_n - \beta_3\omega)\right),$$

$$B = 8(\omega - \beta_3(\bar{k}_n + 1))^2\left(\frac{(\beta_3^2 - 1)\omega_b^2}{(\omega - \beta_3(\bar{k}_n + 1))^2} + 1\right),$$

$\overline{\omega} = \omega/ck_w$, and $\overline{k}_n = k_n/k_w$. This equation describes the coupling between the electrostatic beam mode with the electromagnetic mode. When $k_i \to 0$, uniform ICG (Eq. (38)) is reduced to the well-known helical wiggler dispersion relation.[3]

4. Numerical results and discussion

A numerical study has been made to determine the effects of periodic ion-channel guiding on the electron trajectories and the growth rate of a FEL with helical wiggler. The chosen parameters for this system are characterized by $\gamma = 6$, $\Omega_w = 0.033$, $\lambda_i = 0.13L$, and ω_b is equal to 2.867 and 7.008 for group-I and group-II orbits, respectively.

Figure 1 shows the graph of the normalized axial velocity, $\beta_{\|}$, against ω_i^2 for both uniform ion-channel guiding and periodic ICG for group-I and group-II orbits. An upper bound on the allowed square ion-channel frequency occurs which, for the chosen parameter, is given by $\omega_i^2 < 0.27$ for periodic ICG. In contrast, the solutions corresponding to the group-II orbits occur when $\omega_i > 0$. It is also shown that, the trajectories for group-I and group-II orbits in the presence of periodic ICG shift to the smaller ion-channel frequencies compared with the case of uniform ICG.

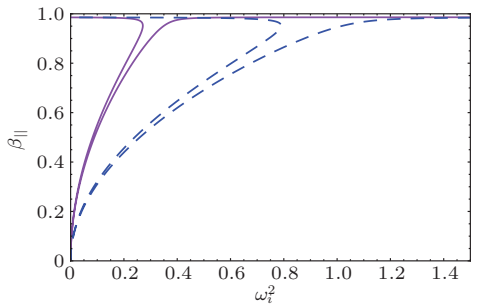


Fig. 1. (color online) Normalized axial velocity as a function of ω_i^2 with a uniform ICG (dashed lines) and periodic ICG (solid lines). The chosen parameters are $\gamma = 6$, $\lambda_i = 0.13L$, and $\Omega_w = 0.033$.

In order to study the effects of periodic ICG on the growth rate, the sixth-order dispersion equation(38), for the complex normalized wave number, $\overline{k}$, has been solved numerically. The growth rate, $\mathrm{Im}(\overline{k})$, as a function of normalized radiation frequency, $\overline{\omega}$, for appropriate values of normalized ion-channel frequency, ω_i, in the presence of periodic ICG for group-I and group-II orbits has been illustrated in Figs. 2(a) and 2(b), respectively. In general, for a given value of ω_i, the growth rate initially increases, rises to a maximum value, and then decreases to zero. It is also shown that the peak growth rate of group-I orbits increases as ω_i increases corresponding to the approach to the resonance, whereas for group-II orbits the growth rate decreases with increasing ω_i. It means that the transverse velocity of the electron increases as the ion-channel frequency approaches the resonance. It should be noted, however, that such enhancements in the transverse velocity correspond to the decrease in the axial velocity of electrons due to the presence of ion channels, and therefore also correspond to the decrease in the resonant frequency of

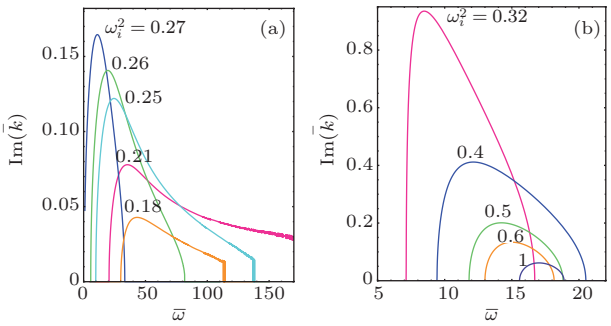


Fig. 2. (color online) Spatial growth rate versus the radiation frequency for periodic ICG for (a) group I (b) for group II orbits. The chosen parameters are $\gamma = 6$, $\Omega_w = 0.03$, $\omega_b = 2.867$ and 7.008 for group I and II orbits, respectively.

interaction. In Fig. 3 the three-dimensional graph of normalized growth rate is plotted as a function of ω_i^2 and $\overline{\omega}$ for uniform ion-channel guiding. It is evident from the results shown in Fig. 3 that the growth rate in the range of $0.14 < \omega_i^2 < 0.4$ remains close to zero, whereas the periodic ion channel (see Fig. 2(a)) has a growth rate in this region (in contrast to the results obtained from the uniform ICG). The periodic ICG has a larger influence on the growth rate than the uniform ICG for group-II orbits. To illustrate this point, we show the normalized growth rate of group-II orbits versus $\overline{\omega}$ for periodic ICG and uniform ICG in Fig. 4. Each curve corresponds to a fixed value of ω_i^2. It is shown that the peak growth rate obtained in a periodic ICG is significantly greater than the maximum growth rate in the uniform ICG, and the range of the radiation frequency is wider.

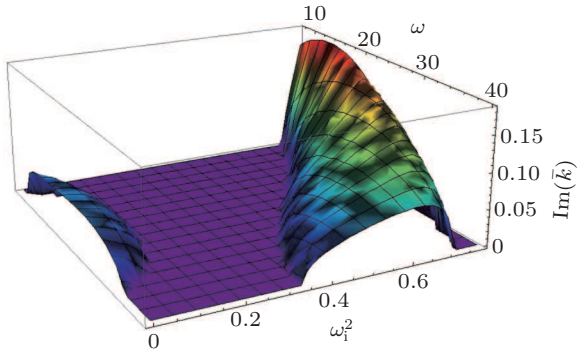


Fig. 3. (color online) Normalized growth rate as a function of normalized resonant frequency $\overline{\omega}$ and normalized ion-channel frequency $\overline{\omega_i}$. The chosen parameters are $\gamma = 6$, $\lambda_i = 0.13L$, $\Omega_w = 0.03$, and $\omega_b = 2.867$ and 7.008 for group-I and group-II orbits, respectively.

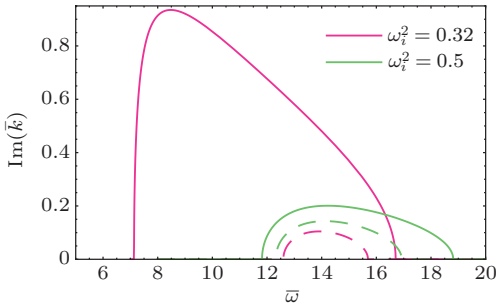


Fig. 4. (color online) Growth rate of instability versus $\overline{\omega}$ for both uniform ICG (dashed lines) and periodic ICG (solid lines). The chosen parameters are $\gamma = 6$, $\lambda_i = 0.13L$, $\Omega_w = 0.03$, and $\omega_b = 2.867$ and 7.008 for group-I and group-II orbits, respectively.

5. Conclusions

In the present paper, the effects of periodic ICG on operation of a FEL configuration with a one-dimensional helical wiggler is investigated. Steady-state trajectories in the single-particle regime are obtained. It is shown that the presence of PICG shifts the resonance frequency to the less magnitude of ion channel frequency. The coupling between the electrostatic beam mode with the electromagnetic mode is described by the sixth-order dispersion equation. It is found that for fixed values of ω_i, as the radiation frequency increases, the spatial linearized growth rate achieves a maximum value, and then decreases to zero. The peak growth rate is obtained as the ion-channel frequency approaches the gyro-resonance frequency. Numerical calculations show that the periodic ICG significantly enhances the growth rate of instability.

References

[1] Takayama K and Hiramatsu S 1988 *Phys. Rev. A* **37** 173

[2] Jha P and Kumar P 1996 *IEEE Trans. Plasma Sci.* **24** 359

[3] Jha P and Kumar P 1998 *Phys. Rev. E* **57** 2256

[4] Su D and Tang C J 2011 *Phys. Plasmas* **18** 023104

[5] Sadegzadeh S, Hasanbeigi A, Mehdian H and Alimohamadi M 2012 *Phys. Plasmas* **19** 023108

[6] Seo Y, Tripathi V K and Liu C S 1989 *Phys. Fluids B* **1** 221

[7] Kurino H, Ebihara K, Hiramatsu S, Kimura Y, Kishiro J, Monaka T, Ozaki T and Takayama K 1990 *Part. Accel* **31** 89

[8] Mehdian H and Raghavi A 2006 *Plasma Phys. Control. Fusion* **48** 991

[9] Lee H C and Jiang T F 2010 *Phys. Plasmas* **17** 113109

[10] Mehdian H, Hasanbeigi A and Jafari S 2010 *Phys. Plasmas* **17** 023112

[11] Raghavi A, Ninno G D and Mehdian H 2008 *Nucl. Instrum. Meth. A* **591** 338

[12] Esmaeilzadeh M, Mehdian H and Willett J E 2002 *Phys. Rev. E* **65** 016501

[13] Jafari B and Maraghechi B 2012 *Phys. Plasmas* **19** 013107

[14] Zhen Y W, Tang C J and Peng X D 2010 *Phys. Plasmas* **17** 083114

[15] Miller J D and Gilgenbach R M 1987 *Phys. Fluids* **30** 3165

[16] Bosch R A and Gilgenbach R M 1988 *Phys. Fluids* **31** 634

[17] Golub Y Y and Rozanov N E 1995 *Tech. Phys.* **40** 346

[18] Hasanbeigi A, Mehdian H and Jafari S 2011 *Chin. Phys. B* **20** 094103